ELSEVIER

Physics of the Earth and Planetary Interiors 95 (1996) 101–122

PHYSICS OF THE EARTH AND PLANETARY INTERIORS

# 3SMAC: an a priori tomographic model of the upper mantle based on geophysical modeling

Henri-Claude Nataf *, Yanick Ricard [1]

*Département Terre-Atmosphère-Océan, URA 1316 du CNRS, École Normale Supérieure, 24 rue Lhomond, 75231 Paris Cedex 05, France*

Received 23 January 1995; revision accepted 21 August 1995

**Abstract**

We present an a priori three-dimensional 'tomographic' model of the upper mantle. We construct this model (called 3SMAC – three-dimensional seismological model a priori constrained) in four steps: we compile information on the thickness of 'chemical' layers in the Earth (water, sediments, upper and lower crust, etc); we get a 3D temperature distribution from thermal plate models applied to the oceans and continents; we deduce the mineralogy in the mantle from pressure and temperature and we finally get a three-dimensional model of density, seismic velocities, and attenuation by introducing laboratory measurements of these quantities as a function of pressure and temperature. The model is thus consistent with various geophysical data, such as ocean bathymetry, and surface heat flux. We use this model to compute synthetic travel-times of body waves, and we compare them with observations. A similar exercise is performed for surface waves and normal modes in a companion paper (Ricard et al., 1996, *J. Geophys. Res.*, in press). We find that our model predicts the bulk of the observed travel-time variations. Both the amplitude and general pattern are well recovered. The discrepancies suggest that tomography can provide useful regional information on the thermal state of the continents. In the oceans, the flattening of the sea-floor beyond 70 Ma seems difficult to reconcile with the seismic observations. Overall, our 3SMAC model is both a realistic model, which can be used to test various tomographic methods, and a model of the minimum heterogeneities to be expected from geodynamical modeling. Therefore, it should be a useful a priori model to be used in tomographic inversions, in order to retrieve reliable images of heterogeneities in the transition zone, which should, in turn, greatly improve our understanding of geodynamical processes in the deep Earth. 3SMAC and accompanying software can be retrieved by anonymous ftp at geoscope.ipgp.jussieu.fr.

## 1. Introduction

### 1.1. The legacy of the first tomographic models

Starting in the 1980s, global tomography has now gained a very large audience. The very first

* Corresponding author.

[1] Present address: Département de Géologie, URA 726 du CNRS, Ecole Normale Supérieure de Lyon, 46 allée d'Italie, 69364 Lyon Cedex 07, France.


*SSDI* 0031-9201(95)03105-7

models of the upper mantle (Nakanishi and Anderson, 1982, 1983, 1984; Woodhouse and Dziewonski, 1984; Nataf et al., 1984, 1986) showed the strong correlation that exists between seismic velocity anomalies and temperature variations associated with plate tectonics. By offering realistic global variations of seismic parameters, they also triggered the development of new seismological theories and methodologies (e.g. Lay and Kanamori, 1985; Jobert, 1987; Tsuboi and Geller, 1989; Lognonné and Romanowicz, 1990). Finally, they revealed anomalous regions, such as the very slow zone in the Red Sea-Afar.

Global models of the lower mantle (Clayton and Comer, 1983; Dziewonski, 1984) had an even larger impact. The large-scale features they pictured were shown to correlate with the geoid. The fact that the correlation seemed to have the wrong sign prompted the development of dynamic models of the mantle (Lago and Rabinowicz, 1984; Richards and Hager, 1984; Ricard et al., 1984). Using the density anomalies deduced from the tomographic models, it became possible to explain for the first time quantitatively the long-wavelength geoid (Richards and Hager, 1984; Ricard et al., 1989). This yielded the idea that the lower mantle was more viscous than the upper mantle by a factor of at least 30.

### *1.2. The flourishing of the recent models*

With the ever increasing amount of high quality data, the improvment of techniques, and the analysis of additional seismic waves, recent models have reached an impressive degree of refinement (e.g. Inoue et al., 1990; Montagner and Tanimoto, 1991; Ekström et al., 1993; Grand, 1994; Su et al., 1994; see Romanowicz, 1991 and Ritzwoller and Lavely, 1995 for a review). These new models appear as one of the main constraints on mantle convection. Strong statements on the style of convection have thus been put forward by seismologists: predominance of large-scale structure (Su and Dziewonski, 1991); organization of the flow in two large upwellings (Montagner and Romanowicz, 1993); deep roots beneath ridges (Su et al., 1992); deep roots beneath cratons (Hara and Geller, 1994; Woodhouse and Dziewonski, 1984; Su et al., 1994); strong degree 2 pattern in the transition zone (Masters et al., 1982). Evidence for low velocities beneath hotspots (Zhang and Tanimoto, 1992; Montagner and Romanowicz, 1993) and for flat lying slabs in the transition zone (Nataf et al., 1986) have also been reported.

It is not clear that all these views are compatible with other geophysical data. Some tomographic models also appear to be mutually incompatible, in particular in the transition zone (Nataf et al., 1986; Romanowicz, 1991). At the same time, voices have arisen to point out limitations and biases of the tomographic techniques (Kawakatsu, 1983; Pulliam and Johnson, 1992; Mochizuki, 1993; Snieder, 1993).

The main goal of this paper is to build an a priori tomographic model of the upper mantle that is compatible with other geophysical data. We then will show how well such a model can predict various seismological data sets. We think that this is a necessary step before new geodynamic constraints can be inferred from seismic tomography.

### *1.3. The importance of crustal corrections*

The shallow Earth is very heterogeneous: crustal thickness varies from almost 0 to 70 km. For surface waves, it was noted very early that the phase velocity variations due to crustal thickness heterogeneities are of the same order as the total observed variations (Nataf et al., 1984). The effect of crustal corrections is also large for body waves. The largest variation is between oceans and continents. This prompted several authors to use a simple ocean/continent correction (M84C in Woodhouse and Dziewonski, 1984). The correction is often assumed to be linear, a somewhat unjustified approximation. One of the goals of this paper is to provide a better crustal model to be used in global seismology.

### *1.4. Heterogeneities of the lithosphere*

One problem with crustal corrections is that they increase the data variance (Montagner and Tanimoto, 1991). The explanation is simple: the crust (slow) is thick over continents, which have a cold (hence fast) uppermost mantle. A laterally

heterogeneous a priori model that includes only crustal variations will therefore provide a worse fit to the data than a radially symmetric a priori model.

Some authors were thus led to propose models that did not include any shallow layer corrections (M84A in Woodhouse and Dziewonski, 1984; Tanimoto, 1990). This is dangerous since we do know that the crust is heterogeneous. A better approach is to include some a priori information on the lithosphere as well as on the crust, so that the a priori model is closer to the actual one. We will argue that the geophysical information we use to build an a priori model of the lithosphere is nearly as reliable as that used to build crustal corrections.

### *1.5. Heterogeneities beneath the lithosphere*

One of the most striking properties of convective systems is that heterogeneities with a large horizontal length scale (in fact the scale of the convective cells) are much larger in the horizontal boundary layers than in the rest of the fluid (Turcotte and Oxburgh, 1967; Jarvis and Peltier, 1986; Honda, 1987). In the mantle, because the viscosity strongly decreases when temperature increases, the largest heterogeneities are found in the upper boundary layer, i.e. the lithosphere (e.g. Richter et al., 1983). Since the vertical resolution of all tomographic methods is rather poor in the upper mantle, the strong variation due to the lithosphere will be smeared vertically, and give rise, in the models, to erroneous deeper heterogeneities. While such heterogeneities might exist (in particular in the transition zone), it is important to assess how large the smearing effect can be, when realistic lithospheric structures are considered. We thus adopt a minimal approach: in our a priori model, we put no heterogeneities beneath the lithosphere, except for slabs and hotspot plumes.

Our goal is to test the validity and limitations of such a three-dimensional seismological model a priori constrained (3SMAC), which includes the minimal heterogeneities revealed by various geophysical, geological, and geochemical observables.

Section 2 describes the general philosophy we follow to build our a priori model. The following sections give the actual approach, values and references, for the various steps used to build 3SMAC-95; 'chemistry' in Section 3, 'temperature' in Section 4, 'mineralogy' in Section 5, and 'constitutive relationships' in Section 6. Section 7 compares several predictions of our model with seismological observations, in particular SS–S and PP–P body wave residual times, as obtained by Woodward and Masters (1991). A more thorough comparison with surface wave data is presented in a companion paper (Ricard et al., 1996).

## 2. General philosophy

Our objective is to build an a priori 3D model of seismologically relevant parameters, in the upper mantle. We propose the following approach. We first 'guess', from various sources, the chemistry at different levels: water, sediments, crust, mantle. We then need to estimate the major thermodynamic parameters that will control the mineralogy and the constitutive relationships of the material. These are pressure and temperature. Pressure is easily related to depth. Much more difficult, and important, is the determination of temperature. We will apply models, introduced to fit heat flux and isostatic topography, in order to derive temperature. Once we know chemistry, pressure, and temperature, we can obtain the mineralogy at all points from experimental phase equilibrium diagrams. Once we know mineralogy, pressure, and temperature, we can calculate the final seismologically relevant parameters (density, P-velocity, S-velocity, quality factor) by injecting experimental measurements of density, seismic velocities and attenuation, as a function of temperature and pressure for all necessary minerals.

Clearly, such an approach is too idealistic to be followed rigorously. For example, there is hardly any experimental data on the variation of elastic and anelastic parameters with pressure, at relevant pressures. On the other hand, our approach is too restrictive: we do not account for anisotropy, in particular. To do so, we would need to infer other non-thermodynamic parameters, such as the strain and stress history of the

material (e.g. Kawasaki, 1986; Estey and Douglas, 1986; Montagner and Nataf, 1986; Ribe, 1989).

As a first step, we will stick to our simple approach, complementing the lack of experimental (or geological) data in various occasions with pragmatic educated guesses. Note that our approach is very similar to that recently applied by De Jonge et al. (1994) at the scale of the Mediterranean region.

### 2.1. Building 3SMAC-95

The model is defined on a $2° \times 2°$ grid, as shown in Fig. 1(a). There are 90 elements in latitude, and 180 in longitude, yielding a total of 16 200 elements. All parameters are constant over each element. The vertical discretization is not regular. Indeed, shallow layers such as ice, water, or sediments, are better described in terms of layers of variable thickness, rather than in lateral variations of parameters at a given depth, the latter being more appropriate for the mantle part of the model. We thus prescribe a stack of predefined shallow layers, as shown in Fig. 1(b). Any of these layers can be empty at a given location. Below level *kstd*, the radii are fixed. The total number of points, and the radii in most of the mantle are therefore constant. Parameters are assumed to vary linearly with radius in each layer.

## 3. Chemistry

Having set the definition of the important 'chemical' layers, the next step is to determine the thickness of these layers over the globe.

### 3.1. Ice (continental)

For Antarctica, we use the compilation of Rand.Sio, as reproduced on the ETOPO5 CDrom (National Geophysical Data Center (NGDC), 1988). For Greenland, we assume that the base of the ice is at a constant altitude of 0 m.

### 3.2. Water and topography

We average the $5' \times 5'$ bathymetry and topography of ETOPO5 (NGDC, 1988) over our grid elements.

### 3.3. Sediments

The data base for sediments is far from being complete. For oceans, we get fairly good coverage by using a compilation established by Colin (1993).

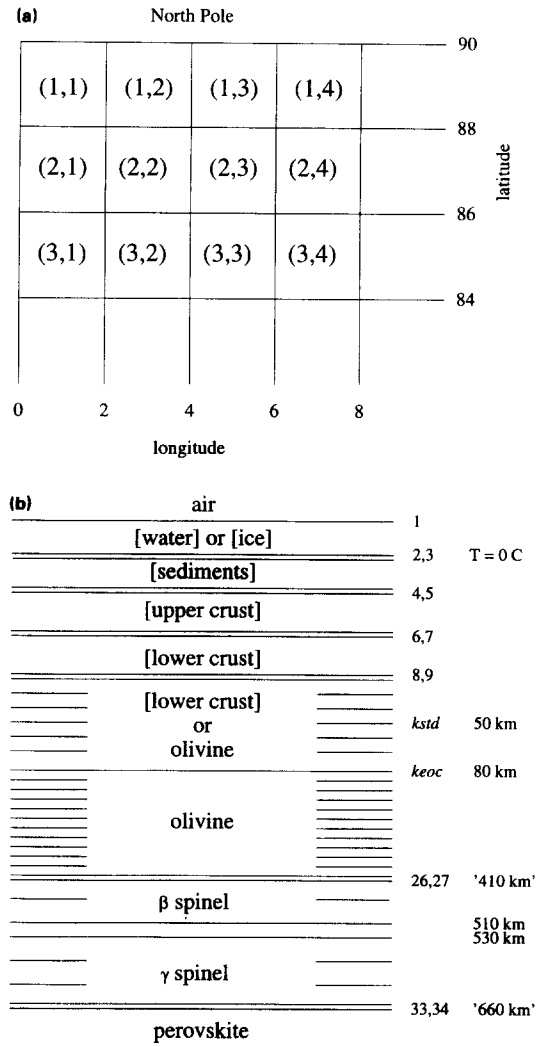


Fig. 1. Sketch of the discretization used to build 3SMAC. (a) Horizontal $2° \times 2°$ grid and indexing. (b) Vertical section. The horizontal boundaries separate layers in which all parameters vary linearly with depth. Double bars mark discontinuities. Vertical indexes are given next to the bars. For indexes *kstd* and larger, the depth of the boundaries are fixed, starting at 50 km. However, the depths of the '410' and '660' km transitions are allowed to vary. Any of the layers in brackets can be empty at a given location. The 0°C isotherm is fixed at the base of the water layer.

It merges data from the Atlantic ocean (Ewing et al., 1973), the Indian oceans (Matthias et al., 1988), and the Pacific ocean (Ludwig and Houtz, 1979), between 71°S and 71°N. In the Pacific ocean, the original data are 2-ways P-wave travel-times. We convert these to thicknesses, using the velocity laws discussed in Section 6. For Eurasia, we use a recent file from Fielding et al. (1993), primarily based on a compilation by Russian scientists (Kunin et al., 1987). For the rest of the continents and continental margins, we constructed a $2° \times 2°$ file from the contours of the Geological World Atlas (1976). Fig. 2 shows our resulting map of sediment thickness.

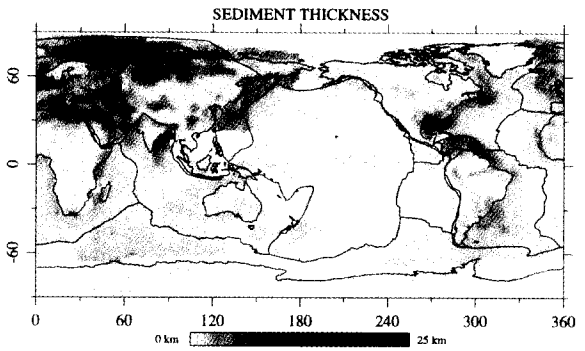


Fig. 2. Map of sediment thickness. Note that the color scale is not linear, in order to accomodate the very small thicknesses in the oceans, and the large ones at continental margins. We have no data for the areas left blank.

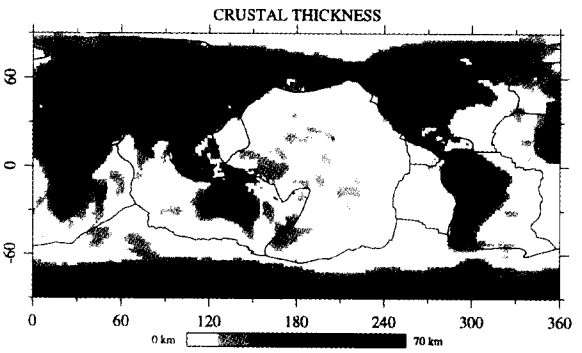


Fig. 3. Map of crustal thickness. This is the thickness of the igneous crust beneath the sediments, when identified. The contour interval is 10 km.

### 3.4. Upper and lower crust

In the oceans, we use the analysis of White et al. (1992) to assign a uniform thickness of 7 km to the igneous crust. In a second step, we perform a correction in order to take into account oceanic plateaus, oceanic island chains, and regions of reduced crustal thickness. The correction is based on the topography analysis of Colin and Fleitout (1990). We convert their 'residual topography' $\delta h$ into crustal thickness variations $\delta H$ with $\delta H = 3\ \delta h$.

In the continents, the points at which crustal thickness is known have a very uneven distribution. This is of concern since the corrections due to crustal variations can be quite significant, for both surface waves and body waves. We start from a $2° \times 2°$ compilation by Cadek and Martinec (1991). This file is based on compilations by Belyaevsky and Volkovsky (1980), Belyaevsky (1981), Allenby and Schnetzler (1983), and Meissner et al. (1987). Over Eurasia, we use the more recent $0.1° \times 0.1°$ compilation of Fielding et al. (1993), averaged over our $2° \times 2°$ grid. We modify crustal thickness over Australia, using data from Dooley and Moss (1988). The resulting map is shown in Fig. 3.

For both oceans and continents, we uniformly ascribe a proportion of 1/3 for the upper crust, with a maximum of 20 km.

### 3.5. Mantle

We consider the mantle to be of uniform chemical composition. Although we have a pyrolitic composition in mind, it does not really matter in our approach, since we will adjust the seismic parameters of the mantle to fit the 'observed' radial seismic models.

## 4. 'Temperature'

Temperature variations in the uppermost mantle are likely to be the main source of seismic heterogeneities. It is therefore crucial to provide realistic temperature profiles.

### 4.1. Oceanic lithosphere

In the oceans, temperature is relatively well constrained by bathymetry and heat flow (Sclater and Francheteau, 1970; Parsons and Sclater, 1977), and modeling (McKenzie, 1967). Plate models have been shown to provide an adequate fit to these data (Parsons and McKenzie, 1978). We use the plate parameters obtained in the most recent study (Stein and Stein, 1992), as listed in Table 1. Although plate models are only an approximation to the actual physics, they contain the important notion that some heat is transported from the mantle to the base of the lithosphere, limiting the half-space cooling trend. They are also appropriate for model testing, since temperature is completely uniform below the chosen base of the plate. We consider that the vertical profile of temperature only depends on the age of the sea floor. We use the recent $0.1° \times 0.1°$ age reconstruction of Müller et al. (1993). This compilation provides no age data for the Mediterranean sea, the circum-Pacific basins nor the polar regions. In our study, it is important that we define these regions as oceanic, even if the ages are not well known. We use various regional studies to delineate the oceanic basins, and get an age estimate. Fig. 4 shows the final age distribution obtained.

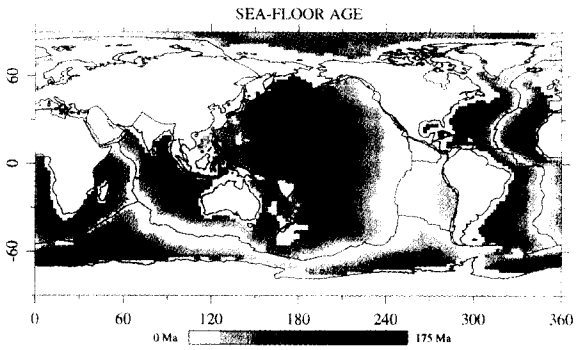


Fig. 4. Map of the age of the sea-floor. Contour interval is 25 Ma.

### 4.2. Continental lithosphere

One of the achievements of global tomography was to show a remarkable correspondence between high velocity regions and old continental cratons (Nakanishi and Anderson, 1982; Woodhouse and Dziewonski, 1984). This is consistent with the idea that the lithosphere is very thick beneath these cratons (Jordan, 1975). Recent heat flow measurements in regions with very low crustal heat production indicate heat flow at the Moho as low as 12 mW $m^{-2}$ (Pinet et al., 1991; Guillou et al., 1994). The continental lithosphere could thicken gradually with age, reaching some asymptotic regime, mainly controlled by the rheology of the mantle constituents (Fleitout and Yuen, 1984; Davaille and Jaupart, 1993). For archean ages, lithospheric thicknesses of 250 km and heat flows of 14 mW $m^{-2}$ have been predicted (Fleitout and Yuen, 1984). Alternatively, it has been proposed that the old continental lithosphere was intrinsically lighter than the 'normal' mantle, due to iron depletion (Jordan, 1975). The thickness of the continental lithosphere could then be controlled by the initial iron depletion. Thicknesses as large as 400 km have been proposed (Lerner-Lam and Jordan, 1987). In most

Table 1
Thermal plate parameters used in 3SMAC

| | Ocean | Tectonic continent | Stable platform | Archean craton |
|---|---|---|---|---|
| Plate thickness $a$ | 95 km | 200 km | 200 km | 300 km |
| Age | – | 100 Ma | 1000 Ma | 2000 Ma |
| Radiogenic temperature $T_{rad}$ | 0 | | 250°C | |
| Radiogenic $e$-depth $z_{rad}$ | – | | 20 km | |
| Thermal diffusivity $\kappa$ | | | $8 \times 10^{-7}$ $m^2$ $s^{-1}$ | |
| Thermal conductivity $k$ | | | 3.14 W $m^{-1}$ $K^{-1}$ | |
| Surface ref. adiabat $T_{ad}^0$ | | | 1350°C | |
| Adiabatic gradient $G_{ad}$ | | | 0.57°C $km^{-1}$ | |

tomographic models, the fast signature of cratons extends at least to 350 km. Here, we will test models in which the continental lithosphere is never thicker than 300 km.

It is very difficult to infer the temperature beneath continents from surface observables. The age of the lithosphere can be very different from the age of the rocks at the surface. Even if the age was well known, the actual temperature profile that should correspond is clearly much more difficult to guess than in the oceans.

We will consider that the temperature distribution can be estimated using a plate model similar to that introduced for the oceanic lithosphere. A slight extension is needed: crustal heat production is taken into account, and we impose that the temperature at the base of a plate is that given by a reference adiabatic profile at the corresponding depth. The expressions for the temperature and heat flux are given in Appendix A.

Bearing in mind that the estimated lithospheric age could be completely wrong in some regions, we have chosen a rather crude regionalization, with only three regions: archean cratons, stable continental platforms, and tectonic regions. Both the age and the plate thickness are assumed constant for a given region, as listed in Table 1. Fig. 5 shows our regionalization. It is based upon the map of Sclater et al. (1980), with modifications in Greenland and in eastern China, where the archean parts have been reduced, in order to account for the observed tertiary volcanism (Laurent Jolivet, personal communication, 1993).

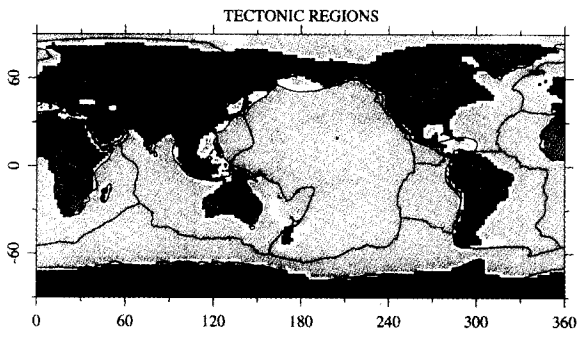


Fig. 5. Regionalization of the continents: tectonic regions in dark; stable platforms in lighter gray; archean cratons in light.

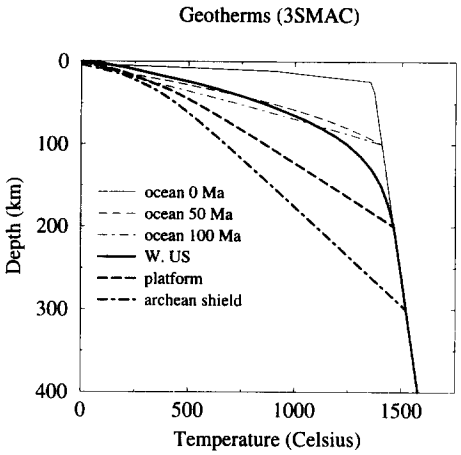


Fig. 6. Geotherms predicted for various typical oceanic and continental regions.

In Fig. 6, we compare the temperature profiles computed for our three continental regions with the oceanic geotherms.

### 4.3. Surface heat flux

One of the first predictions of our model is the distribution of surface heat flux. Fig. 7 compares our computed values with the recent compilation by Pollack et al. (1993). The agreement is very good. One should not be too impressed by this result: the coverage of heat flow measurements is still sparse, especially on continents. Therefore, Pollack's map combines actual measurements with 'predictions' based on these measurements and a regionalization, also relying on the expected age of the lithosphere. However, it is important to note that our thermal model, despite its simplicity, produces the proper range of heat flow values.

The construction of the lithosphere of 3SMAC is now completed, and we turn to deeper thermal heterogeneities. We assume that below the lithosphere, the temperature is adiabatic everywhere, except in slabs and plumes.

### 4.4. Slabs

Slabs of subducted oceanic lithosphere constitute cold patches in the mantle. Assuming that

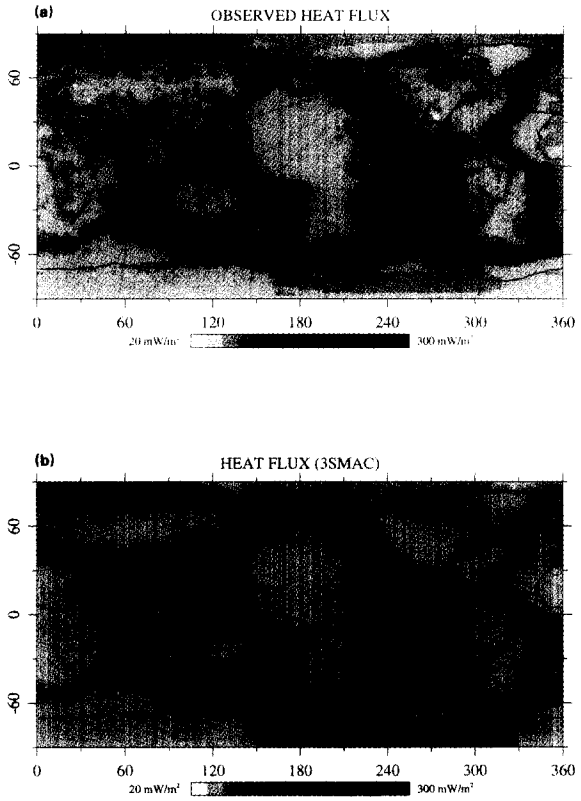


Fig. 7. Surface heat flux. (a) Observed, after Pollack et al. (1993). (b) Predicted from our 3SMAC model. The contour interval is 20 below 100 mW $m^{-2}$, and 50 above. Note the general agreement between the two maps.

the temperature anomaly of the slab mainly diffuses laterally with time, we can determine the horizontally averaged temperature anomaly in the slab (with respect to the adiabatic temperature profile) from the age of the oceanic plate when it entered the mantle (the rate of descent is then irrelevant). The anomaly for one grid cell is therefore simply computed with our oceanic plate model (see Appendix A). Although more thorough analyses have been proposed at the regional scale (De Jonge et al., 1994), they are not necessary at our rather crude level of resolution (2° × 2° grid). We need two types of information: the presence of a slab, and the age (at subduction time) a slab would have had. The latter is crudely derived from the present age of the oceanic plates at the relevant trenches. The presence of a slab is inferred from seismicity: we use the International Seismological Center (ISM) catalog of earthquakes on the time-period 1964 to 1987, available on CD-ROM, to map slabs around the depths 50, 100, 150, 200, 300, 400, 500, 600 km. Fig. 8 shows our slabs at two different depths: 150 and 600 km.

Although there is clear evidence from regional tomography for cold slabs with no seismicity (e.g. Spakman et al., 1988), we stick to our restrictive criterion. Our slab model should therefore be regarded as corresponding to the minimum thermal anomalies associated with subduction. Similarly, we do not include any possible slab-related heterogeneity above or below the 660 discontinuity. In fact, we hope that the use of a realistic model of the uppermost mantle, such as 3SMAC, will enable tomographers to demonstrate the need for such features in the actual Earth.

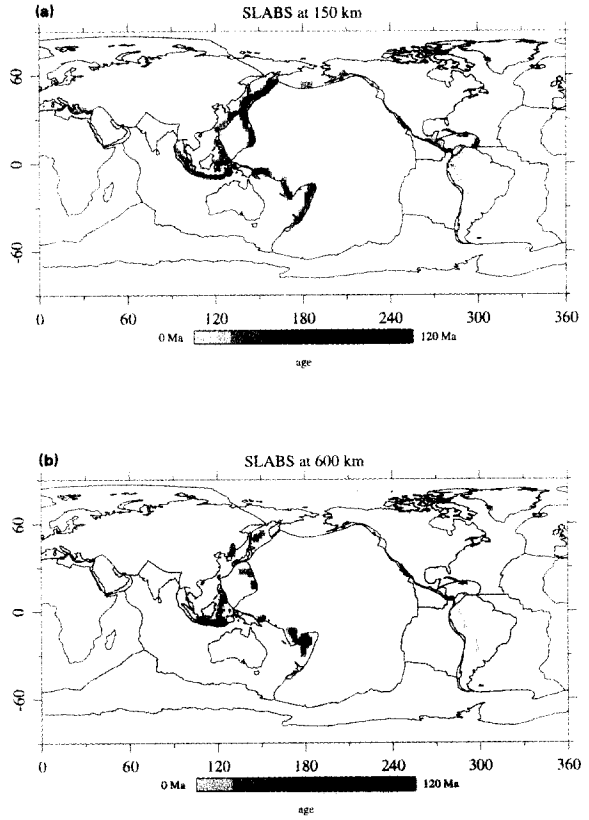


Fig. 8. Maps of subducted slabs, as deduced from seismicity. The shades give the approximate age of the plate when it was subducted. (a) At a depth of 150 km. (b) 600 km.

### 4.5. Hotspot plumes

It is unlikely that narrow hotspot plumes can be detected in global seismic tomography. Plume material spreading beneath the lithosphere could possibly produce a detectable signal, as claimed by Zhang and Tanimoto (1992). Because such a process is not yet well contrained by surface observables, we have not included it in our model. However, for completeness, we have included hotspot plumes, viewed as vertical cylinders of hot material across the upper mantle. We postulate a Gaussian shaped thermal anomaly, with a maximum temperature of 250°C, and a diameter of 150 km for all hotspots (see Nataf and VanDecar, 1993). Our collection of plumes consists of the 47 'standard' hotspots, as listed by Duncan and Richards (1991), plus 50 'new' hotspots detected by Fleitout and coauthors (Fleitout et al., 1989; Fleitout and Moriceau, 1992).

### 4.6. Temperature maps

We now have all the ingredients to calculate the temperature distribution in 3SMAC. Fig. 9 gives our temperature maps at depths of 50, 100, and 500 km. At 50 km, the main features are the cooling of the oceanic plates, and the very cold stable continental regions. At 100 km, the oceans are completely uniform (adiabatic), and we start distinguishing between archean cratons and younger stable platforms. At 500 km, the only anomalies are those associated with subducted slabs and hotspot plumes.

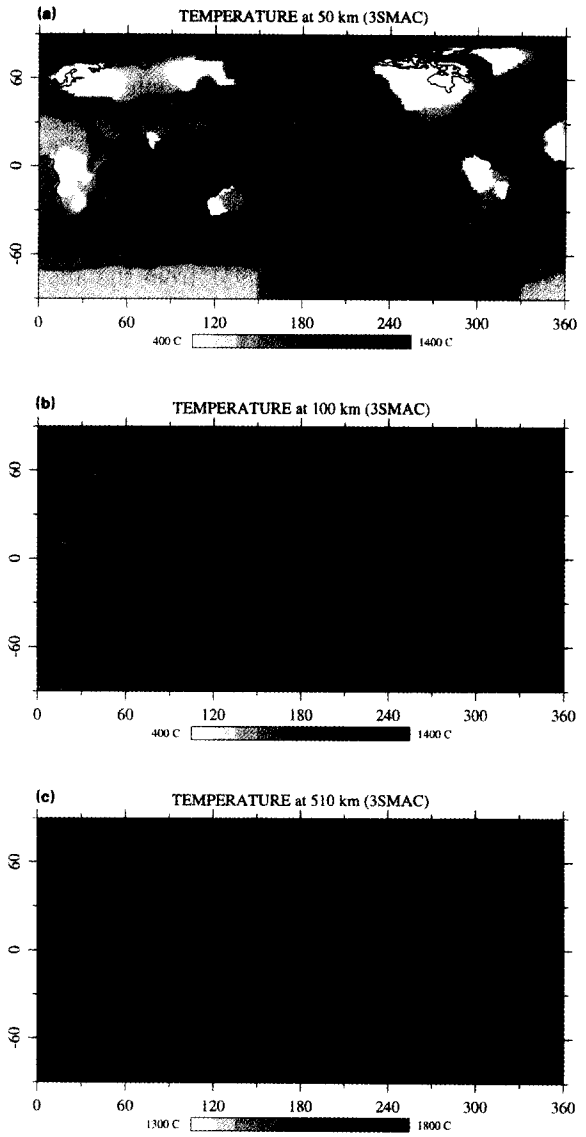


Fig. 9. Maps of predicted temperatures at different depths: (a) 50 km, (b) 100 km, (c) 500 km. Hot regions are in dark, cold regions are light. At 500 km, the only anomalies are those associated to hotspsot plumes and subducted slabs.

## 5. 'Mineralogy'

Once we know chemistry and temperature everywhere in our model, it should be possible to deduce the mineralogy from petrological relationships. Clearly, our 'chemical' mapping is too crude to allow for such a refinement in the crustal layers. However, we should perform this exercise in the mantle part. This simply means that we calculate in what mineralogical phase the mantle is at different depths. We fix the depth of the olivine $\rightarrow$ $\beta$-spinel transition at 410 km, and that of the $\gamma$-spinel $\rightarrow$ perovskite at 660 km, in the 'normal' adiabatic mantle. We then calculate the depth of the transitions in regions will thermal anomalies, using Clapeyron slopes of 3 MPa $K^{-1}$ (Bina and Hellfrich, 1994) for the former, and $-2.5$ MPa $K^{-1}$ (Chopelas et al., 1994) for the

latter. This yields local deflections in the slabs of the order of 24 km up for the 410 km transition, and 18 km down for the 660 km, compatible with observations by Richards and Wicks (1990), and Vidale and Benz (1992). However, when filtered to remove spherical harmonic degrees higher than 8, the deflections are only $\pm 2.5$ km, much smaller than the $\pm 15$ km deduced by Shearer and Masters (1992), and Shearer (1993), from the analysis of S660S reflected waves.

## 6. 'Seismological constitutive laws'

Our final step is to deduce the distribution of the relevant seismological parameters from the distribution of 'chemistry', 'mineralogy', and temperature. We consider the following parameters: density, P-velocity, S-velocity, and the logarithm of the quality factor (which is the inverse of internal dissipation). Remember that anisotropy is not included in 3SMAC. We assume that all these parameters, for a given chemistry and mineralogy, depend upon temperature and pressure according to:

$$X(T, z) = [X_0 + X_z \cdot z] \cdot [1 + X_T \cdot (T - T_{ref})].$$

We choose the reference temperature $T_{ref}$ to be the adiabatic temperature for all mantle mineralogies, and the surface temperature (0°C) for all

Table 2
Physical parameters used to build 3SMAC

| | | $\rho$ | $V_P$ | $V_S$ | ln $Q_\mu$ | Ref. |
|---|---|---|---|---|---|---|
| Water | $X_0$ | 1.02 | 1.45 | 0. | 6. | 1 |
| Ice | $X_0$ | 1. | 4. | 2. | 6. | 2 |
| Oceanic sediments | $X_0$ | 2. | 2.4 | 1.4 | 4.9 | 3 |
| | $X_z$ | 0.08 | 0.2 | 0.1 | 0. | 3 |
| Continental sediments | $X_0$ | 2.6 | 5.5 | 3.0 | 4.9 | 3, 4 |
| | $X_z$ | 0.01 | 0.02 | 0.01 | 0. | 3, 4 |
| Oceanic upper crust | $X_{top}$ | 2.6 | 4.8 | 2.6 | 4.9 | 5 |
| | $X_{bot}$ | 2.85 | 6.0 | 3.2 | 4.9 | 5 |
| | $X_T$ | $-0.4 \times 10^{-4}$ | $-0.8 \times 10^{-4}$ | $-1 \times 10^{-4}$ | 0. | |
| Continental upper crust | $X_{top}$ | 2.7 | 6.0 | 3.5 | 4.9 | 4 |
| | $X_{bot}$ | 2.8 | 6.5 | 3.7 | 4.9 | 4 |
| | $X_T$ | $-0.4 \times 10^{-4}$ | $-0.8 \times 10^{-4}$ | $-1 \times 10^{-4}$ | 0. | |
| Oceanic lower crust | $X_0$ | 2.95 | 6.5 | 3.6 | 4.9 | 5 |
| | $X_z$ | 0.02 | 0.13 | 0.07 | 0. | 5 |
| | $X_T$ | $-0.4 \times 10^{-4}$ | $-0.8 \times 10^{-4}$ | $-1 \times 10^{-4}$ | 0. | |
| Continental lower crust | $X_0$ | 2.85 | 6.5 | 3.8 | 4.9 | 4 |
| | $X_z$ | 0.003 | 0.02 | 0.011 | 0. | 4 |
| | $X_T$ | $-0.4 \times 10^{-4}$ | $-0.8 \times 10^{-4}$ | $-1 \times 10^{-4}$ | 0. | |
| Olivine | $X_0$ | 3.14 | 7.433 | 4.15 | 3.1 | 6, 7, 8 |
| | $X_z$ | $1.06 \times 10^{-3}$ | $3.89 \times 10^{-3}$ | $1.75 \times 10^{-3}$ | $5. \times 10^{-3}$ | 6, 8 |
| | $X_T$ | $-0.33 \times 10^{-4}$ | $-0.9 \times 10^{-4}$ | $-1.1 \times 10^{-4}$ | $-9. \times 10^{-4}$ | 7 |
| $\beta$-spinel and $\gamma$-spinel | $X_0$ | 3.41 | 7.982 | 4.201 | 5.4 | 6, 8 |
| | $X_z$ | $0.88 \times 10^{-3}$ | $3.36 \times 10^{-3}$ | $2.12 \times 10^{-3}$ | 0. | 6, 8 |
| | $X_T$ | $-0.3 \times 10^{-4}$ | $-0.5 \times 10^{-4}$ | $-0.75 \times 10^{-4}$ | $-9. \times 10^{-4}$ | 9 |
| Perovskite | $X_0$ | 3.90 | 9.036 | 4.237 | 5.7 | 6, 8 |
| | $X_z$ | $0.68 \times 10^{-3}$ | $2.66 \times 10^{-3}$ | $2.59 \times 10^{-3}$ | 0. | 6, 8 |
| | $X_T$ | $-0.1 \times 10^{-4}$ | $-0.5 \times 10^{-4}$ | $-0.75 \times 10^{-4}$ | $-9. \times 10^{-4}$ | 9 |

For each chemical/mineralogical 'layer', we derive $X_0$, $X_z$, and $X_T$ (see text). The units are g cm$^{-3}$ for $\rho$, km s for $V_P$ and $V_S$, for the reference value $X_0$. The depth derivative $X_z$ has the same unit divided by km. The logarithmic temperature derivative $X_T$ is in K$^{-1}$. The reference depth is the surface. The reference temperature is 0°C for all non-mantle layers (above the heavy bar), and the temperature of the reference adiabatic profile at that depth for all mantle layers. References: (1) Dziewonski and Anderson (1981). (2) Lliboutry (1965). (3) Hamilton (1976, 1978). (4) Holbrook et al. (1992). (5) White et al. (1992). (6) Kennett and Engdahl (1991). (7) Jackson et al. (1992). (8) Lesage and Valette (1994). (9) karato (1993).

shallower layers. For all considered mineralogies, and all parameters, we thus need the value at zero depth and reference temperature $X_0$, the derivative with respect to depth $X_z$, and the logarithmic derivative with respect to temperature $X_T$.

Table 2 lists the values we adopt, and the sources they come from. Let us insist on a few specific points.

### 6.1. Depth dependence

For the mantle, the pressure derivatives are rarely available at the relevant pressures. They can be extrapolated, using thermodynamic theory, and a precise choice of chemical composition (Duffy and Anderson, 1989; Vacher et al., 1996). Here, we adopt a more pragmatic stand-point: since in our model the mantle is almost entirely adiabatic below 300 km, we deduce the depth derivatives of $V_S$ and $V_P$ from the slopes displayed by the seismological radial model iasp91 (Kennett and Engdahl, 1991). This ensures that our a priori model has the 'correct' parameters in the regions where we predict no thermal heterogeneities. Similarly, the depth variation of density and $\ln Q_\mu$ is taken from the recent reference radial model of Lesage and Valette (1994). However, the reference value of $\ln Q_\mu$ at the surface and adiabatic temperature (1350°C) is deduced from Jackson et al. (1992).

Note that in the upper crust, we do not consider a true depth variation, because the large variation with depth there rather reflects a progression in mineralogy. Therefore, we fix the values of the parameters at the top and bottom, at the reference temperature.

### 6.2. Temperature dependence

Seismic velocity heterogeneities due to temperature variations in the upper 300 km of the mantle (hence in the 'olivine' field) are likely to be the main component of our final model. It is therefore crucial to evaluate the temperature derivatives for 'olivine' as well as possible. These derivatives are available from laboratory experiments for all major minerals of an olivine peridotite. Coefficients for pyrolite and piclogite have been computed by Estey and Douglas (1986). However, it was pointed out by Karato (1993) that these might not be relevant for observed seismic waves, because they are obtained from velocity measurements at ultrasonic frequencies (1 MHz). He noted that, due to internal friction, the derivatives could be up to 100% larger, when estimated at seismic frequencies (1 Hz). A few measurements of shear modulus and internal friction for peridotite at seismic frequencies are now available (Berckhemer et al., 1982; Gueguen et al., 1989; Jackson et al., 1992). We use these data to estimate the following derivatives at our reference frequency of 1 Hz:

$$\frac{1}{V_S}\frac{\partial V_S}{\partial T} = -1.1 \times 10^{-4}\ \mathrm{K}^{-1}$$

$$\frac{1}{V_P}\frac{\partial V_P}{\partial T} = -0.9 \times 10^{-4}\ \mathrm{K}^{-1}$$

$$\frac{1}{\ln Q_\mu}\frac{\partial \ln Q_\mu}{\partial T} = -9 \times 10^{-4}\ K^{-1}.$$

The value for S-velocity is about 50% higher than the ultrasonic one deduced from Estey and Douglas (1986). The value for P-velocity is similar to that derived independently by De Jonge et al. (1994). Note the very strong variation of $Q_\mu$ with temperature: at a depth of 200 km, $Q_\mu = 50$ at the adiabatic temperature, $Q_\mu = 100$ for a temperature 200 K below the adiabat.

### 6.3. Crustal velocities

Because both the composition and the thickness of the crust are so different between oceans and continents, the choice of velocities in the crust will have a profound effect on the overall seismological signature of oceans and continents, especially as seen by body waves. We base our choice on compilations by White et al. (1992) for the oceanic crust, and by Holbrook et al. (1992) for the continental crust. However, it is worth noting that the data for S-wave velocities is very sparse. Dispersion of short-period surface waves would be of great help in constraining that part of our model (Trampert and Woodhouse, 1995).

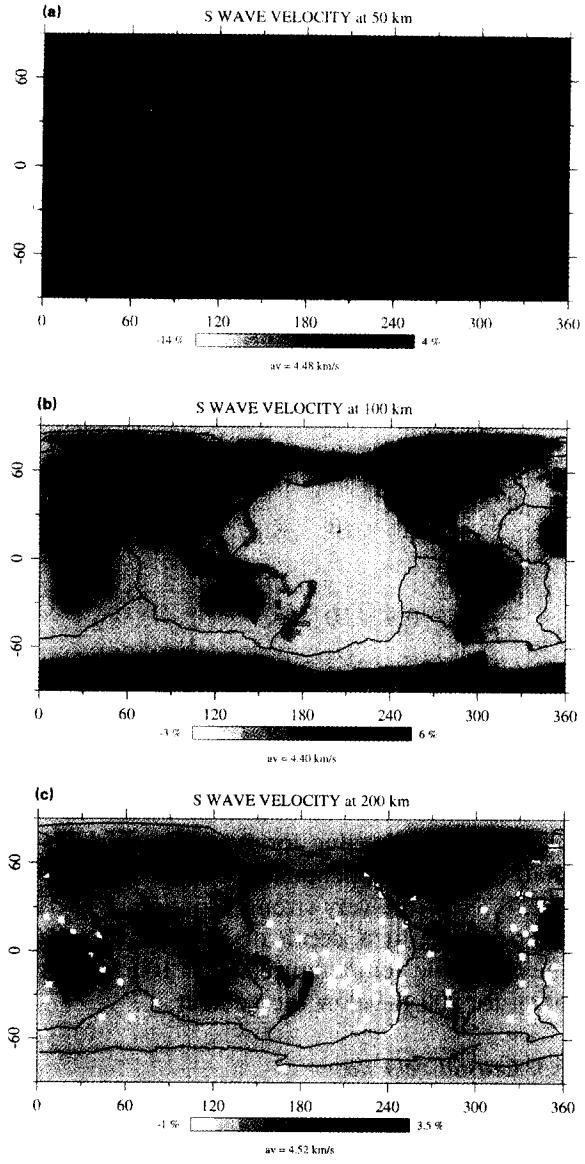


Fig. 10. Maps of predicted S-wave velocities at different depths (a) 50 km, (b) 100 km, (c) 200 km. We plot the percentage variations from the average value (given below the legend). The contour interval is 1% for (a) and (b), and 0.5% for (c).

## 7. 3SMAC predictions

Fig. 10 shows maps of S-velocity heterogeneities in model 3SMAC at depths of 50, 100, and 200 km. Note the strong signature of the East-Pacific ridge at 50 km, with anomalies up to 6%. At 100 km, the only anomalies are those associated with continents, with amplitudes up to 6%. Fig. 11 shows the same thing for the quality factor $Q_\mu$. Note the strong variations, with $Q_\mu$ as low as 20 beneath ridges, and up to 400 beneath archean cratons.

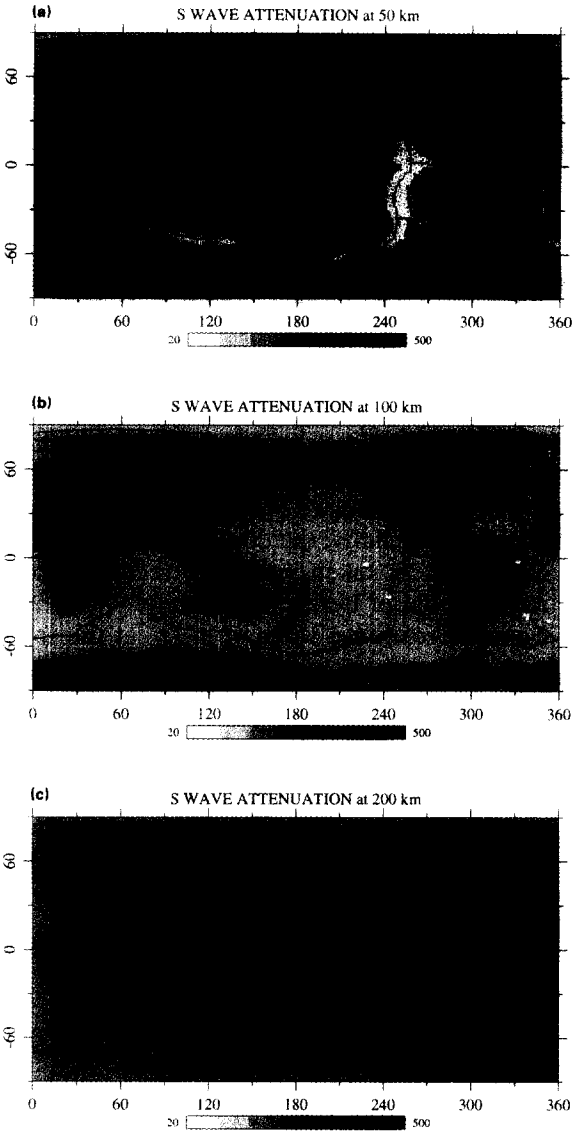


Fig. 11. Maps of predicted quality factor $Q_\mu$ for S-waves at different depths: (a) 50 km, (b) 100 km, (c) 200 km. The color scale is logarithmic. Each contour corresponds to a multiplication of $Q_\mu$ by a factor of 1.5.

### 7.1. Comparisons with regional seismic profiles

Velocity profiles have been derived for both P- and S-waves for various tectonic regions. In particular, Helmberger and his many students have produced quite a collection of models, deduced from the trial-and-error fit of waveforms of waves that interact with the upper mantle discontinuities (Walck, 1984; Grand and Helmberger, 1984a,b; Graves and Helmberger, 1988; LeFevre and Helmberger, 1989; Zhao and Helmberger, 1993). This technique probably provides the best depth resolution of all seismological methods (see also Lerner-Lam and Jordan, 1987), with the drawback that the structure is assumed to be

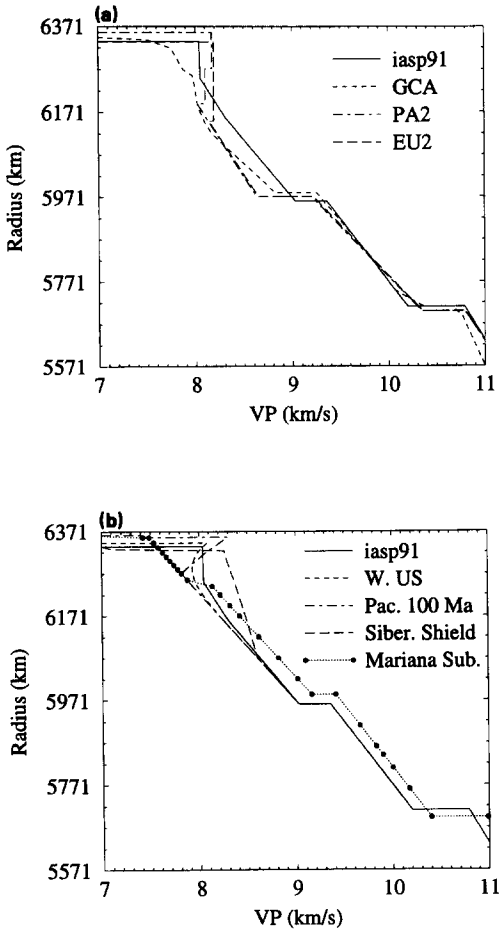


Fig. 12. Comparisons between our predicted seismic profiles in various regions with 'observed' profiles, for P-waves. The iasp91 model (Kennett and Engdahl, 1991) is plotted in both graphs. (a) 'Observed' seismic models: GCA (Gulf of California) from Walck (1984), PA2 (100 Ma Pacific Ocean) and EU2 (Eurasian shield) from Lerner-Lam and Jordan (1987). (b) Predicted seismic profiles in 3SMAC: they can be compared directly with the corresponding observed profiles. The profile 'Mariana Sub.' is for a subducting slab.

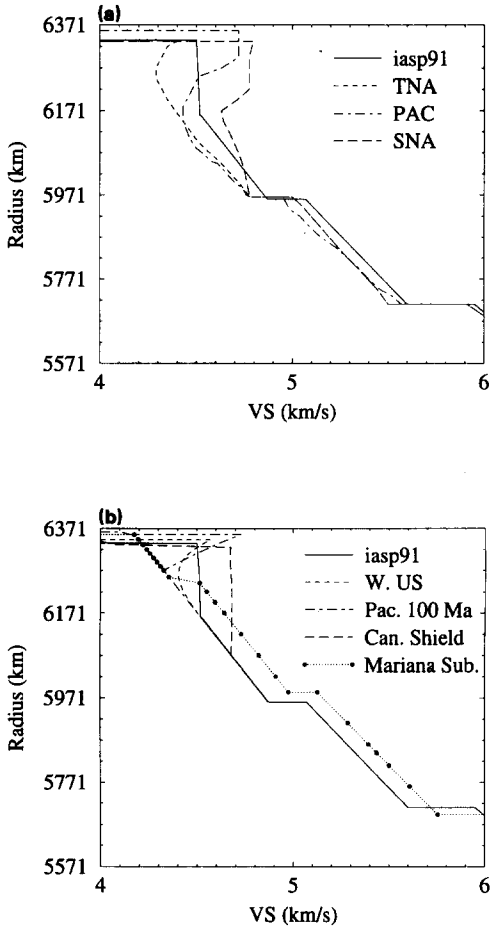


Fig. 13. Same as Fig. 12, but for S-waves. The 'observed' seismic models are: TNA (Gulf of California and W. US) and SNA (Canadian shield) from Grand and Helmberger (1984a) and PAC (100 Ma Pacific Ocean) from Graves and Helmberger (1988).

laterally homogeneous over several thousands of kilometers.

In Fig. 12, we compare P-velocity profiles predicted by our model in various regions with these 'observed' profiles. Three observed profiles are shown in Fig. 12(a): the GCA model of Walck (1984) was derived for the Gulf of California, PA2 (Lerner-Lam and Jordan, 1987) is for a part of the Pacific Ocean with ages around 100 Ma, and EU2 (Lerner-Lam and Jordan, 1987) is a model for the Eurasian shield. Average model iasp91 (Kennett and Engdahl, 1991) is also drawn

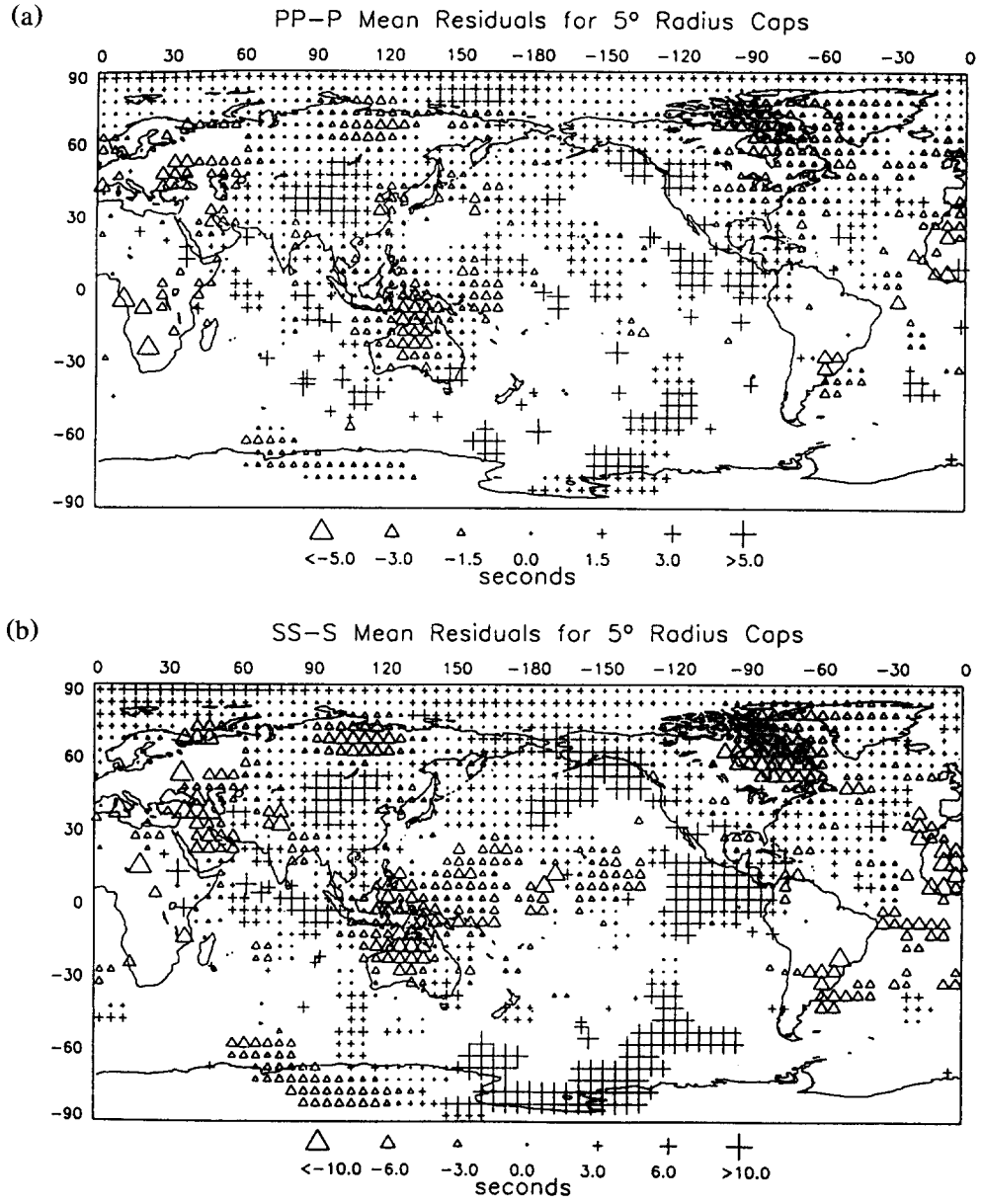


Fig. 14. Maps of observed PP–P (a) and SS–S (b) travel-time residuals plotted at the surface bounce point of PP (or SS). From Woodward and Masters (1991).

for reference. In Fig. 12(b), we draw the profiles obtained from our model for the same regions: western US, 100 Ma-old ocean, and Siberian shield. We observe that the range of predicted variations is similar to the observed one. However, we predict very steep negative velocity gradients in the oceans. It would be interesting to test such models against actual observations. In

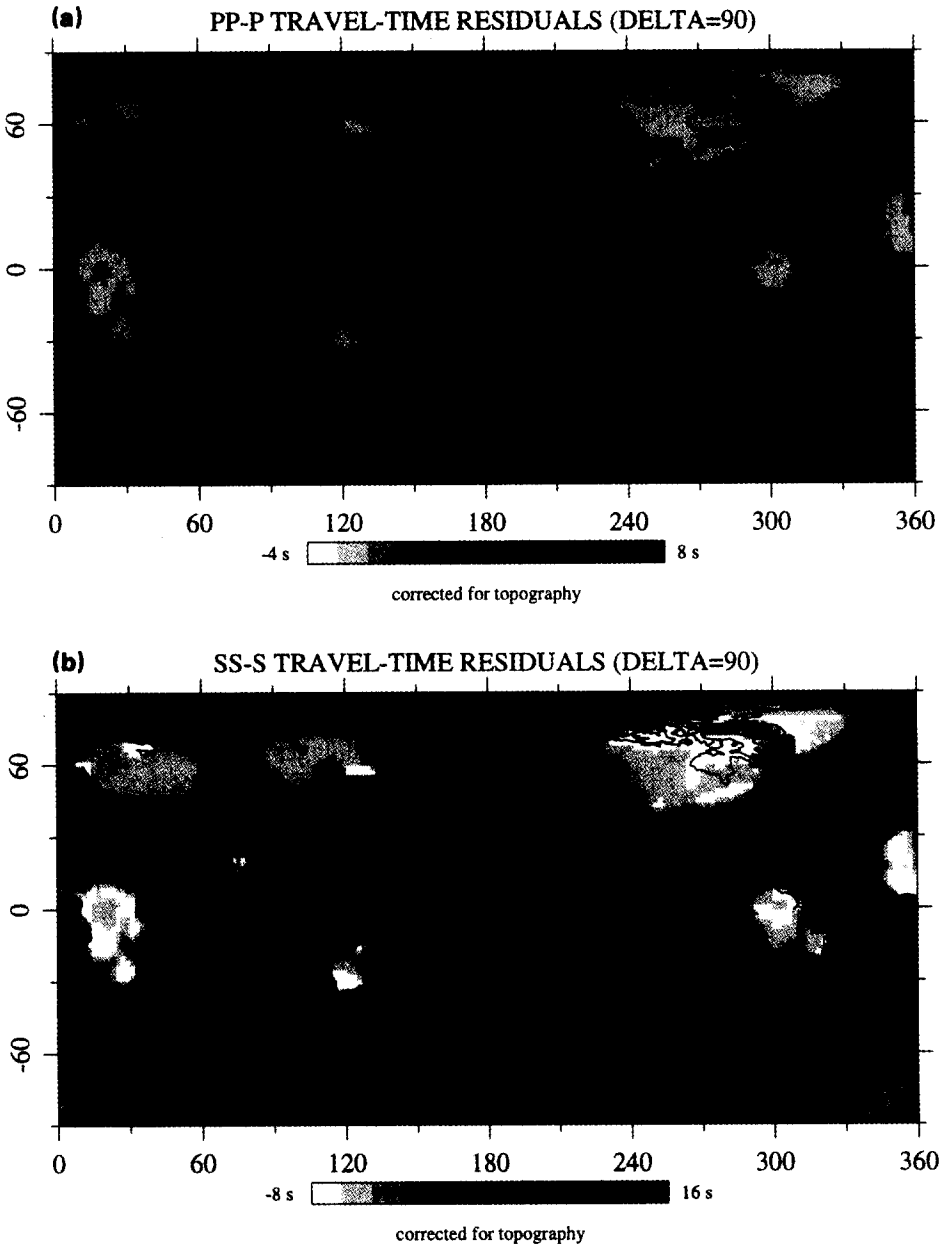


Fig. 15. Maps of travel-time residuals predicted by our a priori 3D tomographic model 3SMAC. (a) PP–P residuals plotted at the surface bounce point of PP (for a hypothetical epicentral distance $\Delta = 90°$, and a period of 25 s). The contour interval is 1 s. (b) Same for SS–S. Contour is 2 s. The residuals are corrected for topography, for direct comparison with those of Fig. 14.

these regions, our model has no heterogeneity below 300 km, in contrast with the 'observed' profiles. For comparison, we also plot in Fig. 12(b) the profile we predict for the Mariana subduction zone. The cold slab produces large velocities at all depths (except near the surface, because the oceanic age at the surface happens to be zero), and deflections of the 410 and 660 km discontinuities.

Fig. 13 performs a similar comparison for S-waves. Three observed profiles are shown in Fig. 13(a): The TNA model of Grand and Helmberger (1984a) was derived for the western US and Gulf of California, PAC (Graves and Helmberger, 1988) is for a part of the Pacific Ocean with ages around 100 Ma, and SNA (Grand and Helmberger, 1984a) is a model for the archean Canadian shield.

### 7.2. *Comparisons with global maps of travel-times*

Woodward and Masters (1991) have obtained SS–S and PP–P residual travel-times from the analysis of long-period digital seismograms. Assuming that most of the residual is due to heterogeneities in the upper mantle beneath the surface bounce point of SS (or PP), they have produced maps such as those shown in Fig. 14. Making the same assumption, we can calculate similar travel-time anomalies, as predicted with our model. We set up a method, described in Appendix B, to compute residual travel-times that take into account changes in the ray geometry due to the heterogeneities. Fig. 15 shows our predicted PP–P and SS–S travel-time anomalies, computed for an epicentral distance of 90°, and corrected for topography for direct comparison with those of Woodward and Masters. Both the amplitudes and the patterns of the heterogeneities are rather well reproduced.

In the continents, the slowest region is the Tibetan plateau, with SS delays up to 7 s, while the archean shields are the fastest, with delays of −6 s, in good agreement with the observations. In detail, there are a number of discrepancies, with observed 'shield-like' values, where we expect younger signatures, and vice-versa. In the oceans, the total predicted variations are about 5 s, smaller than the observed ones. Fig. 16 shows the variation of the SS–S residuals (corrected for topography) as a function of the square root of

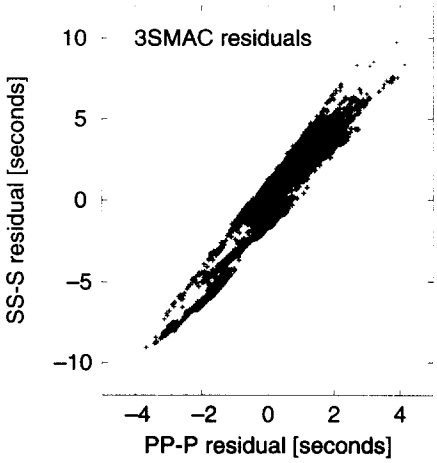


Fig. 17. SS–S versus PP–P residuals (corrected for topography) predicted by 3SMAC. This plot can be compared with Fig. 13 of Woodward and Masters (1991). We obtain a very similar correlation, with $\delta t_{SS-S} \approx 2.5\ \delta t_{PP-P}$.

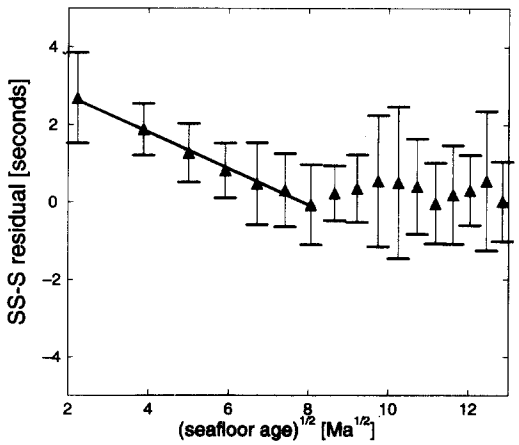


Fig. 16. Variations of SS–S residuals (corrected for topography) predicted from 3SMAC, as a function of the square root of the age of the sea-floor. We plot the mean and the standard deviation of the data on 5 Ma bins. This result can be compared with Fig. 19 of Woodward and Masters (1991), except that they plot the standard deviation of the mean (about ten times smaller than that of the data (G. Masters, personal communication, 1994)). The fit to data for ages less than 64 Ma is almost exactly the same at theirs.

age for all oceans. The plot can be compared with Fig. 19 of Woodward and Masters (1991). Again, the predicted total variation is less than the observed one, but we note that the fit to ages less than 70 Ma is $-0.47$ s $Ma^{-1/2}$, almost the same value ($-0.51$) as reported by Woodward and Masters. The deficit of negative delays in our model is essentially due to the lack of variations beyond 70 Ma, a consequence of the plate model we use (Stein and Stein, 1992).

We obtain similar results for PP–P residuals. Fig. 17 is a plot of SS–S residuals versus PP–P residuals (both corrected for topography) from our model. it can be compared with Fig. 13 of Woodward and Masters. We obtain a very similar range of values. The two types of residuals are strongly correlated, with $\delta t_{SS-S} \approx 2.5\delta t_{PP-P}$, in good agreement with the observations.

## 8. Conclusion

We have derived an a priori 'tomographic' three-dimensional model of the upper mantle, using information from many different branches of the Earth sciences. Special attention was given to crustal thickness variations, which contribute significantly to lateral heterogeneities as seen by body waves and surface waves. Most of the remaining lateral variations in these data sets can be attributed to temperature variations in the uppermost mantle. We have used a 'plate model' to predict the profiles of temperature versus depth beneath oceans (as a function of age) and continents. Our model and accompanying software can be obtained through anonymous ftp to geoscope.ipgp.jussieu.fr. We welcome further input and comments to improve this model.

Assuming a variation of S-velocity with temperature 50% higher at seismic frequencies (1 Hz) than experimentally derived at ultrasonic frequencies (1 MHz), we predict lateral variations in S-velocities that are in very good agreement with those deduced from the observations of SS–S travel-time anomalies (Woodward and Masters, 1991). A similar agreement is obtained for PP–P anomalies, the two being correlated. The predicted correlation $\delta t_{SS-S} = 2.5\delta t_{PP-P}$ is very similar to the observed one.

In the oceans, the variation with age of SS–S delays predicted by 3SMAC is very similar to the one obtained from observations by Woodward and Masters (1991). However, the plate model we use (Stein and Stein, 1992) produces no variation for ages larger than about 70 Ma, in contrast to the observations. This suggests that the oceanic plate continues to thicken with age at old ages, or that cold blobs detached from the lithosphere (Agnon and Lyakhovsky, 1995) are seen by the SS waves. Alternatively, the SS waves might be seeing deeper structure, in the transition zone, which is not included in our model. On the other hand, the data do not seem to require any 'active' upwelling beneath ridges.

All these tests suggest that our model, based on the knowledge we have of crustal variations, and on the minimal thermal anomalies we can infer from geodynamical modeling, accounts for the bulk of the observed heterogeneities in the upper mantle. We therefore argue that it can be used as a realistic model to test various tomographic inversions. Such tests performed on surface waves and normal modes are presented in a companion paper (Ricard et al., 1996). We also think that 3SMAC can be used as an a priori model for future tomographic inversions. Clearly, there is more in the Earth than what we put in 3SMAC, and that missing part is the interesting one! We think that starting from this minimal, yet realistic, model will improve the resolution of the deeper heterogeneities.

3SMAC can be improved in a number of ways. There is a lack of data on S-velocities in the crust. The dispersion of short-period surface waves could bring some useful information. Ages and temperatures beneath continents are difficult to obtain. It is probably in this domain that regional tomography can contribute most. More generally, we think that an international effort of compilation of additional data could lead to an improved a priori model.

## Acknowledgements

This study benefited from suggestions and data from many people. We thank in particular O.

Cadek, P. Colin, M.-P. Doin, E. Engdahl, E. Fielding, L. Fleitout, Ph. Huchon, L. Jolivet, Ph. Lognonné, B. Kennett, S. Lallemant, Ph. Lesage, G. Masters, J.-P. Montagner, H. Pollack, B. Valette, and A. Zielhuis. We thank Steve Grand for a very detailed and constructive review, and an anonymous referee for taking the time to read our manuscript. The maps were plotted with program 'P' developed by Spakman, Govers, de Jonge and Remkes at the University of Utrecht. This research was supported by INSU–CNRS 'Tomographie'.

## Appendix A. Temperature profile in a plate with crustal heat production and adiabatic background

The classical plate model (McKenzie, 1967; Stein and Stein, 1992) assumes that the temperature $T_{base}$ at the base of the plate is fixed. The thickness $a$ of the plate is also fixed, as well as the plate velocity $U$ in the $x$ direction. The initial vertical temperature profile is $T(t=0, z)=T_{base}$. Sclater and Francheteau (1970) proposed two extensions: the initial vertical profile is an adiabat, and radiogenic heat production $H$ is present in the plate. One then solves the heat equation:

$$\frac{\partial T}{\partial t}+U\frac{\partial T}{\partial x}=\kappa\left(\frac{\partial^2 T}{\partial x^2}+\frac{\partial^2 T}{\partial z^2}\right)+\frac{H}{\rho C_p}$$

where $\kappa=k/\rho C_p$ is the heat diffusivity, $k$ is the thermal conductivity, $\rho$ density, and $C_p$ heat capacity.

The initial vertical temperature profile follows the adiabat, given by:

$$T_{ad}=T_{ad}^0+G_{ad}z.$$

The temperature imposed at the base of the plate is also the 'adiabatic' one:

$$T_{base}=T_{ad}(z=a).$$

In order to treat the case of the continents, we assume that the volume heat production is of the form:

$$H(z)=H_0e^{-z/z_{rad}}$$

we characterize $H_0$ by the temperature increase $T_{rad}$ it yields at the base of the radiogenic layer at long times:

$$T_{rad}=\frac{H_0 z_{rad}^2}{k}.$$

We then derive the following steady-state solution (neglecting horizontal heat diffusion):

$$T(t,z)=T_{base}\left\{\frac{z}{a}+\frac{T_{rad}}{T_{base}}\left[1-\frac{z}{a}\cdot(1-\varepsilon_0)-e^{-z/z_{rad}}\right]\right.$$
$$+\sum_{n=1}^{\infty}\frac{2}{n\Pi}\left[1-\frac{G_{ad}a}{T_{base}}-\frac{T_{rad}}{T_{base}}\cdot\frac{1-\varepsilon_n}{1+\left(n\Pi\frac{z_{rad}}{a}\right)^2}\right]$$
$$\left.\times\exp\left(-n^2\Pi^2\frac{\kappa t}{a^2}\right)\sin\left(n\Pi\frac{z}{a}\right)\right\}$$

with $\varepsilon_0=e^{-a/z_{rad}}$, which is often small, and $\varepsilon_n=(-1)^n\varepsilon_0$.

The heat flux at the surface becomes:

$$q(t)=\frac{kT_{base}}{a}\left\{1+\frac{T_{rad}}{T_{base}}\left(\frac{a}{z_{rad}}-1+\varepsilon_0\right)\right.$$
$$+2\sum_{n=1}^{\infty}\left[1-\frac{G_{ad}a}{T_{base}}-\frac{T_{rad}}{T_{base}}\cdot\frac{1-\varepsilon_n}{1+\left(n\Pi\frac{z_{rad}}{a}\right)^2}\right]$$
$$\left.\times\exp\left(-n^2\Pi^2\frac{\kappa t}{a^2}\right)\right\}.$$

In the absence of internal heat production, the thermal anomaly averaged over the thickness of the plate is:

$$\frac{1}{a}\int_0^a[T(t,z)-T_0(z)]\cdot dz$$
$$=-\frac{T_{base}}{2}\cdot\left(1-\frac{G_{ad}a}{T_{base}}\right)\left[1-\frac{8}{\Pi^2}\sum_{\substack{n=1\\ n\ \text{odd}}}^{\infty}\frac{1}{n^2}\right.$$
$$\left.\times\exp\left(-n^2\Pi^2\frac{\kappa t}{a^2}\right)\right]$$

## Appendix B. Quasi 1D body wave travel times with some effect of ray geometry

We want to compute travel-time anomalies in our 3SMAC model. The simplest quasi 1D way to do so is to integrate along a given ray the slowness vertical profile for each $2° \times 2°$ cell of our horizontal grid. This assumes that the ray sees the same vertical distribution during its trip in the heterogeneous uppermost mantle. This assumption is certainly violated in columns with hotspots or slabs, but is quite reasonable to describe the longer wavelength features, such as ocean versus cratons, and so on.

But what ray should we choose? For a given epicentral distance $\Delta$, one would classically choose the ray given by a reference model. We can be more realistic by letting the ray be bent in the heterogeneous region. We thus choose a ray parameter value $p_0$ (the one which yields the appropriate $\Delta$ in the reference model), we trace (1D) the ray in the heterogeneous uppermost mantle (down to 350 km), and compute its travel time $t$ and epicentral increment $\delta$. We then continue the ray with the same ray parameter in the radial reference model. The total epicentral distance $\Delta'$ is usually different from the required one, and we iterate on the ray parameter $p$ to get the proper value.

With this method, we can assess in a self-consistent fashion the error made by assuming that SS and S rays (for example) are affected by the heterogeneous structure beneath the station in a similar way. This assumption is the basis for all differential phase studies, such as SS–S, ScS–S, PP–P, etc. For an epicentral distance of 90°, we find that the maximum error is only $\pm 0.5$ s for SS–S, to be compared with the total anomaly of $\pm 8$ s, due to structure at the SS surface bounce point. This confirms the validity of the approximation used in differential studies. However, we note that the pattern of errors is very systematic, with negative errors over cratons, and positive ones in young oceans.

## References


Agnon, A. and Lyakhovsky, V., 1995. Oceanic topography and heat flow: indications for a silent discharge of cold rock into the convective Earth. Geophys. Res. Lett., 22: 1273–1276.

Allenby, R.J. and Schnetzler, C.C., 1983 United States crustal thickness. Tectonophysics, 93: 13–31.

Belyaevsky, N.A., 1981. Structure of the Earth Crust from Geologic–Geophysical Data. Nedra, Moscow (in Russian).

Belyaevsky, N.A. and Volkovsky, I.S., 1980. Tectonic map of Northern Eurasia. Relief of the Moho surface, Moscow.

Berckhemer, H., Kampfmann, W., Aulbach E. and Schmeling, H., 1982. Shear modulus and Q of forsterite and dunite near partial melting from forced oscillation experiments. Phys. Earth Planet. Inter., 29: 30–41.

Bina, C.R. and Hellfrich, G., 1994. Phase transition Clapeyron slopes and transition zone seismic discontinuity topography. J. Geophys. Res., 99: 15853–15860.

Cadek, O. and Martinec, Z., 1991. Spherical harmonic expansion of the earth's crustal thickness up to degree and order 30. Studia Geoph. Geod., 35: 151–165.

Chopelas, A., Boehler, R. and Ko, T., 1994. Thermodynamics and behavior of $\gamma$-$Mg_2SiO_4$ at high pressure: implications for $Mg_2SiO_4$ phase equilibrium, Phys. Chem., 21: 351–359.

Clayton, R.W. and Comer, R.P., 1983. A tomographic analysis of mantle heterogeneities from body wave travel times. EOS Trans. AGU, 62: 776 (abstract).

Colin, P., 1993. Geoïde global; topographie associée et structure de la convection dans le manteau terrestre: modélisation et observations. Thèse de Doctorat, Université Paris 7.

Colin, P. and Fleitout, L., 1990. Topography of the ocean floor: thermal evolution of the lithosphere and interaction of deep mantle heterogeneities with the lithosphere. Geophys. Res. Lett., 11: 1961–1964.

Davaille, A. and Jaupart C., 1993 Transient high Rayleigh number thermal convection with large viscosity variations. J. Fluid Mech., 253; 141–166.

De Jonge, M.R., Wortel, M.J.R. and Spakman, W., 1994. Regional scale tectonic evolution and the seismic velocity structure of the lithosphere and upper mantle: The Mediterranean region. J. Geophys. Res., 99: 12091–12108.

Dooley, J.C. and Moss, F.J. 1988. Deep crustal reflections in Australia 1957–1973 – II. Crustal models. Geophys. J. Int., 93: 239–249.

Duffy, T.S. and Anderson, D.L., 1989. Seismic velocities in mantle minerals and the mineralogy of the upper mantle, J. Geophys. Res., 94: 1895–1912.

Duncan, R.A. and Richards, M.A., 1991. Hotspots, mantle plumes, flood basalts and true polar wander. Rev. Geophys., 29: 31–50.

Dziewonski, A.M., 1984. Mapping the lower mantle. J. Geophys. Res., 89: 5929–5952.

Dziewonski, A.M. and Anderson, D.L., 1981. Preliminary Reference Earth Model. Phys. Earth Planet. Inter., 25: 297–356.

Ekström, G., Tromp, J. and Larson, E.W., 1993. Measurements and models of global surface wave propagation. Trans. Am. Geophys. Un., 74: 438 (abstract).

Estey, L.H. and Douglas, B.J., 1986. Upper mantle anisotropy: a preliminary model, J. Geophys. Res., 91: 11393–11406.

Ewing, M., Carpenter, G., Windisch, C. and Ewing, J., 1993. Sediment distribution in the oceans: the Atlantic. Geol. Soc. Am. Bull., 84: 71–88.

Fielding, E.J., Barazanghi M. and Isacks, B.L., 1993. A geological and geophysical database for Eurasia, Final Technical Report, Phillips Laboratory, Hanscom AFB, Massachussets, USA, 38 pp.

Fleitout, L. and Moriceau, C., 1992. Short-wavelength geoid, bathymetry, and the convective pattern beneath the Pacific Ocean. Geophys. J. Int., 110: 6–28.

Fleitout, L. and Yuen, D.A., 1984. Secondary convection and the growth of the oceanic lithosphere. Phys. Earth Planet. Inter., 36: 181–212.

Fleitout, L., Dalloubeix, C. and Moriceau, C., 1989. Small-wavelength geoid and topography anomalies in the South Atlantic ocean: a clue to new hotspot tracks and lithospheric deformation. Geophys. Res. Lett., 16: 637–640.

Geological World Atlas, 1976. Coordinators Choubert and Faure-Muret, UNESCO, Paris.

Grand S.P., 1994. Mantle shear structure beneath the Americas and surrounding oceans. J. Geophys. Res., 99: 11591–11621.

Grand, S.P. and Helmberger, D.V., 1984a. Upper mantle shear structure of North America. Geophys. J. Royal Astron. Soc., 76: 399–438.

Grand, S.P. and Helmberger, D.V., 1984b. Upper mantle shear structure beneath the Northwest Atlantic Ocean. J. Geophys. Res., 89: 11465–11475.

Graves, R.W. and Helmberger, D.V. 1988. Upper mantle cross-section from Tonga to Newfoundland. J. Geophys. Res., 93: 4701–4711.

Gueguen, Y., Darot, M., Mazot P. and Woirgard, J., 1989. $Q^{-1}$ of forsterite single crystals. Phys. Earth Planet. Inter., 55: 254–258.

Guillou, L., Mareschal, J.-C., Jaupart, C., Gariepy, G., Bienfait G. and Lapointe, R., 1994. Heat flow, gravity and structure of the Abitibi belt, Superior Province, Canada: implications for mantle heat flow. Earth Planet. Sci. Lett., 122: 103–123.

Hamilton, E.L., 1976. Variations of density and porosity with depth in deep-sea sediments. J. Sedim. Petrol., 46: 280–300.

Hamilton, E.L., 1978. Sound velocity–density relations in sea-floor sediments and rocks. J. Acoust. Soc. Am., 63, 366–377.

Hara, T. and Geller, R.J., 1994. The geological origin of long wavelength lateral heterogeneity at depths of 300–400 km. Geophys. Res. Lett., 21: 907–910.

Holbrook, W.S., Mooney W.D. and Christensen, N.I., 1992. The seismic velocity structure of the deep continental crust. In: D.M. Fountain, R. Arculus and R.W. Kay (Editors) Continental Lower Crust, Elsevier, pp. 1–43.

Honda, S., 1987. The rms residual temperature in the convecting mantle and seismic heterogeneities. J. Phys. Earth, 35: 195–207.

Inoue, H., Fukao, Y., Tanabe, K. and Ogata, Y., 1990. Whole mantle P-wave travel time tomography, Phys. Earth Planet. Inter., 59, 294–328.

Jackson, I., Patterson M.S. and Fitz Gerald, J.D. 1992. Seismic wave dispersion and attenuation in Aheim dunite: an experimental study, Geophys. J. Int., 108: 517–534.

Jarvis, G. and Peltier, W., 1986. Lateral heterogeneity in the convecting mantle, J. Geophys. Res., 91: 435–451.

Jobert, N., 1987. Mantle wave deviations from 'pure-path' propagation on aspherical models of the Earth by Gaussian beam waveform analysis, Phys. Earth Planet. Inter., 47: 253–266.

Jordan, T.H., 1975. The continental tectosphere, Rev. Geophys. Space Phys., 13: 1–12.

Karato, S., 1993. Importance of anelasticity in the interpretation of seismic tomography, Geophys. Res. Lett., 20: 1623–1626.

Kawakatsu, H., 1983. Can 'pure-path' models explain free oscillation data? Geophys. Res. Lett., 10: 186–189.

Kawasaki, I., 1986. Azimuthally anisotropic model of the oceanic upper mantle. Phys. Earth Planet. Inter., 43: 1–21.

Kennett, B. and Engdahl, E.R. 1991. Traveltimes for global earthquake location and phase identification. Geophys. J. Int., 105: 429–465.

Kunin et al. 1987. Institute of Physics of the Earth, Moscow maps.

Lago, B. and Rabinowicz, M. 1984. Admittance for a convection in a layered spherical shell, Geophys. J. Royal Astron. Soc., 77: 461–482.

Lay, T. and Kanamori, H. 1985. Geometric effects of global lateral heterogeneity on long-period surface wave propagation. J. Geophys. Res., 90: 605–621.

LeFevre, L.V. and Helmberger D.V., 1989. Upper mantle P velocity of the Canadian shield. J. Geophys. Res., 94: 17749–17765.

Lerner-Lam, A.L. and Jordan, T.H., 1987. How thick are the continents? J. Geophys. Res., 92: 14007–14026.

Lesage, Ph. and Valette, B., 1994. Improving spherical earth models, (*abstract*) Meeting of the European Geophysical Society, Ann. Geophys., supply 1 to Vol. 12, p. C76 (abstract).

Lliboutry, L.A., 1965. Traité de Glaciologie, Masson, Paris.

Lognonné, Ph. and Romanowicz, B., 1990. Modelling of coupled normal modes of the earth: the spectral method. Geophys. J. Int., 102; 365–395.

Ludwig, W.J. and Houtz, R.E., 1979. Isopach map of sediments in the Pacific Ocean basin and marginal sea basins, Am. Assoc. Pet. Geol. Rep.

Masters, G., Jordan, T.H., Silver, P.G., and Gilbert, F., 1982. Aspherical earth structure from fundamental spheroidal mode data. Nature, 298: 609–613.

Matthias, P.K., Rabinowitz, P.D. and Dipiazza, N., 1988. Sediment thickness map of the Indian Ocean, Map 505, AM. Assoc. Pet. Geol., Tulsa, USA.

McKenzie, D.P., 1967. Some remarks on heat flow and gravity anomalies. J. Geophys. Res., 72: 6261–6273.

Meissner R., Wever, Th. and Flüh, E.R., 1987. The Moho in

Europe–Implications for crustal development, Ann. Geophys., 5B: 357.

Montagner, J.-P. and Nataf, H.-C., 1986. A simple method for inverting the azimuthal anisotropy of surface waves, J. Geophys. Res., 91: 511–520.

Montagner, J.-P. and Romanowicz B., 1993. Degrees 2, 4 and 6 inferred from seismic tomography, Geophys. Res. Lett., 20: 631–634.

Montagner, J.-P. and Tanimoto T., 1991. Global upper mantle tomography of seismic velocities and anisotropies. J. Geophys. Res., 96: 20337–20351.

Mochizuki, E. 1993. Spherical harmonic analysis in terms of line integral, Phys. Earth Planet. Inter., 76: 97–101.

Müller, R.D., Roest, W.R., Royer, I.-Y., Gahagan, L.M. and Sclater, J.G. 1993. A digital map of the ocean floor. Scripps Institution of Oceanography Reference Series No. 93-30.

Nakanishi, I. and Anderson, D.L. 1982. World-wide distribution of group velocity of mantle Rayleigh waves as determined by spherical harmonic inversion. Bull. Seismol. Soc. Am., 72: 1185–1194.

Nakanishi, I. and Anderson D.L., 1983. Measurements of mantle wave velocities and inversion for lateral heterogeneity and anisotropy, 1, Analysis by the single-station method, J. Geophys. Res., 88: 10267–10284.

Nakanishi, I. and Anderson D.L., 1984. Measurements of mantle wave velocities and inversion for lateral heterogeneity and anisotropy, 2, Analysis by the single-station method, Geophys. J. Royal Astron. Soc., 78: 573–618.

Nataf, H.-C. and VanDecar, J., 1993. Seismological detection of a mantle plume? Nature, 364: 115–120.

Nataf, H.-C., Nakanishi, I. and Anderson, D.L., 1984. Anisotropy and shear-velocity heterogeneities in the upper mantle, Geophys. Res. Lett., 11; 109–112.

Nataf, H.-C., Nakanishi I. and Anderson D.L., 1986. Measurements of mantle wave velocities and inversion for lateral heterogeneities and anisotropy. 3. Inversion. J. Geophys. Res., 91: 7261–7307.

National Geophysical Data Center (NGDC), 1988. ETOPO-5 Bathymetry/Topography data, Data announcement 88-MGG-02: National Oceanic and Atmospheric Administration, US Department of Commerce.

Parsons, B. and McKenzie, D.P., 1978. Mantle convection and the thermal structure of the plates, J. Geophys. Res., 83: 4485–4496.

Parsons, B. and Sclater J.G., 1977. An analysis of the variation of ocean floor bathymetry and heat flow with age. J. Geophys. Res., 82: 803–827.

Pinet, C., Jaupart, C., Mareschal J.-C., Gariepy, C., Bienfait, G. and Lapointe R., 1991. Heat flow and structure of the lithosphere in the eastern part of the Canadian Shield. J. Geophys. Res., 96: 1941–1964.

Pollack, H.N., Hurter, S.J. and Johnson, J.R., 1993. Heat flow from the Earth's interior: analysis of the global data set. Rev. Geophys., 31: 267–280.

Pulliam, R.J. and Johnson L.R., 1992. What pattern of heterogeneity in the Earth's mantle can be revealed by seismic travel time tomography? Phys. Earth Planet. Inter., 73: 109–151.

Ribe, N.M., 1989. Seismic anisotropy and mantle flow. J. Geophys. Res., 94: 4213–4223.

Ricard, Y., Fleitout L. and Froidevaux, C., 1984. Geoid heights and lithospheric stresses for a dynamical earth. Ann. Geophys., 2: 267–286.

Ricard, Y., Vigny, C. and Froidevaux, C., 1989. Mantle heterogeneities, geoid and plate motions: a Monte-Carlo inversion J. Geophys. Res., 94: 13739–13754.

Ricard, Y., Nataf, H.-C. and Montagner, J.-P., 1996. 3-dimensional seismological model a priori constrained: confrontation with seismic data. J. Geophys. Res., in press.

Richards, M.A. and Hager, B.H., 1984. Geoid anomalies in a dynamical earth. J. Geophys. Res., 89: 5987–6002.

Richards, M.A. and Wicks Jr., C.W., 1990 S–P conversion from the transition zone beneath Tonga and the nature of the 670 km discontinuity. Geophys. J. Int., 101: 1–35.

Richter, F.M., Nataf, H.-C. and Daly, S.F., 1983. Heat transfer and horizontally averaged temperature of convection with large viscosity variations. J. Fluid Mech., 129: 173–192.

Ritzwoller, M.H. and Lavely, E.M., 1995. Three dimensional seismic models of the Earth's mantle. Rev. Geophys., 33: 1–66.

Romanowicz, B., 1991. Seismic tomography of the Earth's mantle. Ann. Rev. Earth Planet. Sci., 19: 77–99.

Sclater, J.G. and Francheteau, J. 1970. The implications of terrestrial heat-flow observations on current tectonics and geochemical models of the crust and upper mantle of the Earth. Geophys. J. Royal Astron. Soc., 20: 509–542.

Sclater, J.G., Jaupart, C. and Galson, D., 1980. The heat flow through oceanic and continental crust and the heat loss of the Earth. Rev. Geophys. Space Phys., 18: 269–311.

Shearer, P.M., 1993. Global mapping of upper mantle reflectors from long-period SS precursors. Geophys. J. Int., 115: 878–904.

Shearer, P.M. and Masters, T.G., 1992. Global mapping of topography on the 660-km discontinuity. Nature, 355: 791–796.

Snieder, R., 1993. Global inversions using normal modes and long-period surface waves. In: H.M. Iyer and K. Hirahara (Editors). Seismic Tomography: Theory and practice, Chapman Hall, London, pp. 23–63.

Spakman, W., Wortel, M.J.R. and Vlaar, N.J., 1988. The Hellenic subduction zone: a tomographic image and its geodynamic implications. Geophys. Res. Lett., 15: 60–63.

Stein, C.A. and Stein, S., 1992. A model for the global variation in oceanic depth and heat flow with lithospheric age. Nature, 359: 123–129.

Su, W.-J. and Dziewonski, A.M., 1991. Predominance of long-wavelength heterogeneity in the mantle. Nature, 352: 121–126.

Su, W.-J., Woodward, R.J. and Dziewonski, A.M., 1992. Deep origin of mid-oceanridge seismic velocity anomalies. Nature, 360: 149–152.

Su, W.-J., Woodward, R.J. and Dziewonski, A.M., 1994. Degree 12 model of shear velocity heterogeneity in the mantle. J. Geophys. Res., 99: 6945–6980.

Tanimoto, T., 1990. Long wavelength S-wave velocity structure throughout the mantle. Geophys. J. Int., 100: 327–336.

Trampert, J. and Woodhouse, J.H., 1995. Global phase velocity maps of Love and Rayleigh waves between 40 and 150 s. Geophys. J. Int., 122: 675–690.

Tsuboi, S. and Geller, R.J., 1989. Coupling between the multiplets of laterally heterogenous earth models. Geophys. J. Int., 96: 371–379.

Turcotte, D.J. and Oxburgh, R.E., 1967. Finite amplitude convection cells and continental drift. J. Fluid Mech., 28: 29—42.

Vacher, P., Mocquet, A. and Sotin, C., 1996. Comparisons between tomographic structures and models of convection in the upper mantle. Geophys. J. Int., 124: 45–56.

Vidale, J.E. and Benz, H.M. 1992. Upper-mantle seismic discontinuities and the thermal structure of subduction zones. Nature, 356: 678–683.

Walck, M.C., 1984. The P-wave upper mantle structure beneath an active spreading centre: the Gulf of California. Geophys. J. Royal Astron. Soc., 76: 697–723.

White, R.S., McKenzie, D.P. and O'Nions, R.K., 1992. Oceanic crustal thickness from seismic measurements and rare earth element inversions. J. Geophys. Res. 97: 19683–19715.

Woodhouse, J.H. and Dziewonski, A.M., 1984. Mapping the upper mantle: three-dimensional modeling of earth structure by inversion of seismic waveforms. J. Geophys. Res., 89: 5953–5986.

Woodward R.L. and Masters, G., 1991. Global upper mantle structure from long period differential travel times, J. Geophys. Res., 96: 6351–6377.

Zhang, Y.-S. and Tanimoto, T., 1992. Ridges, hotspots and their interaction as observed in seismic velocity maps. Nature, 355: 45–49.

Zhao, L.-S. and Helmberger, D.V., 1993. Upper mantle compressional velocity structure beneath the northwest Atlantic ocean. J. Geophys. Res., 98: 14185–14196.